

Generic FRI-Based DOA Estimation: A Model-Fitting Method

Yongfei Li, Ruiming Guo , Thierry Blu , *Fellow, IEEE*, and Hangfang Zhao

Abstract—Direction of arrival (DOA) estimation is a classical topic in source localization. Notably, a reliable grid-free sparse representation algorithm, called FRI (finite rate of innovation) algorithm, was proposed to recover the finite number of Dirac pulses from a stream of 1D temporal samples, which also offers a efficient solution to the DOA estimation problem. Typically, FRI method assumes uniform sampling with single snapshot. However, the actual situation is richer and more diverse. Motivated by the requests of practical applications (e.g. array deployment, algorithm run-speed, etc.), a generic FRI method is proposed to tackle the more general case in practice, i.e. non-uniform sampling with multiple snapshots. Instead of annihilating the measured sensor data, a model-fitting method is used to robustly retrieve the sparse representation (i.e. DOAs and associated amplitudes) of the 1D samples. We demonstrate that our algorithm can handle challenging DOA tasks with high-resolution, which we validate in various conditions, such as multiple coherent sources, insufficient signal snapshots, low signal-to-noise ratio (SNR), etc. Moreover, we show that the computational complexity of our algorithm mainly scales with the number of sources and varies very slowly with the number of samples and snapshots, which meets the needs of a wider range of practical applications.

Index Terms—Finite rate of innovation (FRI), direction of arrival (DOA), high-resolution, multiple snapshots, non-uniform sampling.

I. INTRODUCTION

DOA estimation is a classical topic in array signal processing, and it plays an important role in many disciplines, with application examples ranging from sonar and radar detection, mobile communication, to GPS (global positioning system) services, as shown in Fig. 1. In this paper, we consider the

far-field scenario where the sources are sufficiently far away and the sensor array is linear with narrowband processing. In order to focus on the weak sources, the SNR is defined for each individual source. Due to the Rayleigh threshold, conventional beamforming (CBF) suffers from low resolution and large sidelobes, resulting in unsatisfactory performance in the presence of multiple sources. In order to address this issue, some high-resolution methods, such as the minimum-variance distortionless response (MVDR) [1], [2], the multiple signal classification (MUSIC) [3], the estimating signal parameter via rotational invariance techniques (ESPRIT) [4] and compressive sensing (CS) [5], [6], [7], [8], [9] have been developed with significant performance improvements.¹

Although these methods have achieved great success in some application scenarios, there are still unresolvable problems in practice. The first challenge is coherent sources. Two sources are coherent if their amplitudes are statistically correlated [10]. This source coherence leads to the degradation of the rank of the built covariance matrix [11], which brings about estimation inaccuracy when using these covariance-based techniques (e.g. MVDR, MUSIC, and ESPRIT, etc.). The second difficulty in practice is weak source measurements with very few snapshots. Many covariance-based techniques [1], [12], [13], [14], essentially rely on sufficient snapshot data to ensure the robustness and accuracy of DOA estimation [5], especially in the presence of low signal-to-noise ratio. However, in some applications like mobile source localization, only very few snapshots are available, which tremendously restricts the accuracy of these techniques. The next challenge is non-uniform sampling. In practice, lots of application situations in DOA estimation is data absence of the uniform sensor array, which eventually gives rise to non-uniform (i.e. sub-sampled) measurements [15], [16], [17]. In this paper, we refer to sub-sampling as non-uniform sampling in terms of the common practical application requirements [18], [19]. This non-uniform circumstances frequently occur in data collection and causes relatively large error in DOA estimation when applying the existing techniques (e.g. CBF, MVDR, MUSIC, etc.) [2].

Another increasingly important issue in many practical applications is the computational cost of the DOA estimation algorithm [20]–[23]. Nowadays, more and more DOA-related tasks require fast run-speed to enable various instant services, like indoor logistic tracking [24], environmental sensing [25]

Manuscript received February 5, 2021; revised May 11, 2021 and June 13, 2021; accepted June 17, 2021. Date of publication June 28, 2021; date of current version August 3, 2021. This work was supported in part by the National Key R&D Program of China under Grant 2016YFC 1400100, in part by the Science and Technology on Sonar Laboratory under Grants 6142109190202 and 6142109KF2018, and in part by the Research Grants Council of Hong Kong under Grant AoE/M-05/12. (*Corresponding author: Hangfang Zhao.*)

Yongfei Li is with the College of Information Science and Electronic Engineering, Zhejiang University, Hangzhou, Zhejiang 310007, China (e-mail: liyongfei@zju.edu.cn).

Hangfang Zhao is with the College of Information Science and Electronic Engineering, Zhejiang University, Hangzhou, Zhejiang 310007, China, with the Laboratory of Ocean Observation-Imaging Testbed of Zhejiang Province, Zhoushan, Zhejiang 316021, China, with the Engineering Research Center of Oceanic Sensing Technology and Equipment, Ministry of Education, Zhoushan, Zhejiang 316021, China, and also with the State Key Laboratory of Fluid Power and Mechatronic Systems, Zhejiang University, Hangzhou, Zhejiang 310007, China (e-mail: hfzhao@zju.edu.cn).

Ruiming Guo and Thierry Blu are with the Department of Electronic Engineering, Chinese University of Hong Kong, Shatin 999077, Hong Kong (e-mail: 1155100873@link.cuhk.edu.hk; thierry.blu@m4x.org).

Digital Object Identifier 10.1109/TSP.2021.3092344

¹All figures in Fig. 1 are selected from Google Image: <https://www.google.com/imghp?hl=en>

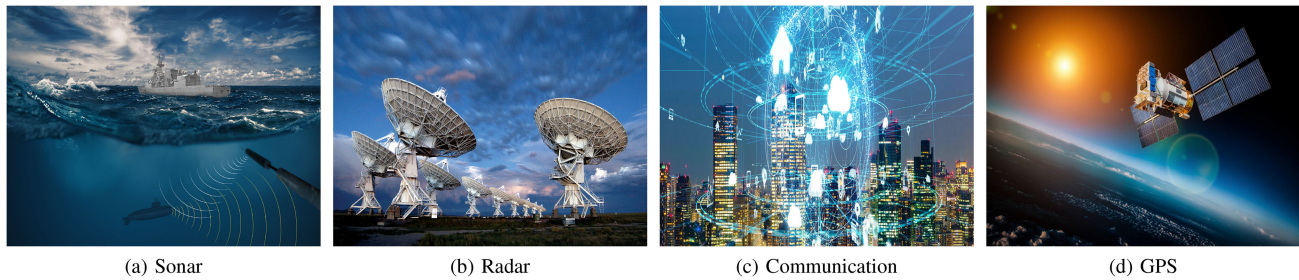


Fig. 1. A wide range of potential applications for DOA estimation. (a) Underwater localization (sonar). (b) Target detection (radar). (c) Wireless communication. (d) Satellite navigation (GPS).

and traffic surveillance [26]. However, many high-resolution DOA estimation algorithms (e.g. CS, etc.) rely on dense grid to guarantee the required estimation precision [27], [28], which is time-consuming and prohibited in practice.

In order to solve the practical problems in DOA-related tasks, a faster and more robust high-resolution DOA estimation algorithm is needed. Note that a reliable method called FRI (Finite Rate of Innovation) [29] shows this potential, which focus on the perfect recovery of the nonbandlimited signals. This is because the bandlimited signals can be acquired through sampling and perfectly recovered from the measured samples in accordance with Shannon sampling theorem. What are less obvious are sampling schemes utilizing some sort of sparsity in the nonbandlimited signal, and this is the central theme of the FRI work. Namely, instead of general bandlimited signals, we focus on the sampling of classes of nonbandlimited signals. This makes it possible to evade Nyquist and exactly sample and recover signals exploiting sparse sampling, at a rate characterized by how sparse they are per unit of time [29]. In some sense, the 1D signal is sampled at its rate of innovation by applying the Law of Parsimony (Occam's razor principle). From an algorithmic point of view, finding the innovations of a nonbandlimited signal and retrieving the DOAs from the spatial sinusoids are one and two sides [30]–[34].

The classic FRI approach utilizing Cadzow denoising is designed for uniform temporal samples, and achieves good performance despite the presence of strong noise [31]. Moreover, in order to address the non-uniform (i.e. irregularly sampled) measurements in radioastronomy, a generalized FRI technique based on annihilation filter was developed that unifies a variety of FRI-based methods [30], [35]–[39]. The algorithms developed for that purpose, in principle, can be used in our context. However, even if they are sufficiently general to retrieve frequencies of noisy non-uniform samples, they are not robust enough to handle some practical DOA problems. The main reason is that the available sensor measurements in practice are sufficiently far apart in space [40], [41], which does not satisfy the hypothesis of densely sampled measurements of these algorithms. Besides, many real DOA data is acquired from uniform sensor array with data absence at known sensor nodes [18], [19]. This extra information could be utilized to further improve the accuracy and robustness of DOA estimation. Apart from these factors, the computational complexity of these non-uniform FRI algorithms depends on the number of sensor nodes, which is not

fast enough when tackling multiple snapshot sensor data in practice.

Recently a new FRI algorithm based on a ratio-structure model that represents the DFT of a sum of sinusoids as ratio of two polynomials, is proposed for high resolution and fast run-speed [42], [43]. The computational complexity of this FRI algorithm essentially only scales with the number of sources, not the number of sensor samples. However, this algorithm only applies to the uniform measurements with single snapshot, which does not meet the needs of practical DOA estimation applications. Motivated by this, we propose a generic FRI algorithm for DOA estimation with multiple snapshots and non-uniform (sub-sampled) measurements: “ss-FRI algorithm”. The contribution of this work can be summarized as follows:

- 1) Use ratio-structure model instead of annihilating filter. The computational cost of the proposed ss-FRI algorithm merely scales with number of sources independent of the number of sensor samples and data snapshots, which significantly improves the run-speed of the DOA estimation (see Section IV-D and Section V-B4).
- 2) Extend the single-snapshot FRI algorithm to multiple snapshots. A more general ratio-structure model is developed to jointly perform model-fitting on the multiple snapshot sensor data, leading to a more accurate and efficient DOA estimation (see Section V-B2).
- 3) Extend the uniform FRI algorithm to non-uniform sampling. A new sub-sampling ratio-structure model is proposed to directly perform model-fitting on the non-uniform sensor measurements, which gives rise to a very robust DOA estimation even in conditions of strong noise and insufficient sensor measurements (see Section V-A3).

This paper is organized as follows. The ratio-structure FRI framework aimed at uniform samples with single snapshot is briefly reviewed, and then further extended to multiple snapshots in Section II. In Section III, we first give the problem formulation of non-uniform sampling, and then develop a more general ratio-structure model that represents the non-uniform measurements as the ratio of two polynomials. We present the algorithmic implementation and computational complexity of our ss-FRI algorithm in Section IV. We validate our ss-FRI algorithm in various conditions, both on substantial simulations (Section V) and real DOA data (Section VI). We conclude the paper by summarizing our main results and highlighting the potential of this method in practical applications in Section VII.

Note that the curly parentheses notation $\{\cdot\}$ denotes a vector or matrix in this paper.

II. SS-FRI DOA ESTIMATION FOR ULAS

A. Single Snapshot ss-FRI DOA Estimation

Signal Model for Single Snapshot. Given a ULA (uniform linear array) with N sensors, for the narrowband sources, the complex envelope representation of the received signal of the n -th sensor generated by K sources is given by [2]

$$y_n = \sum_{k=1}^K x_k e^{-j2\pi \frac{d}{\lambda} n \sin \theta_k}, \quad n = 0, 1, \dots, N-1 \quad (1)$$

where d is the element interval, λ is the wavelength, x_k is the complex amplitude, and $\sin \theta_k$ is the DOA (direction of arrival) of the k -th source (DOA refers to $\sin \theta_k$ instead of θ_k in this paper.).

Now, in noisy conditions (i.e. additive white noise), the DOA estimation can be formulated as the following sinusoid fitting problem:

$$\min_{x_k, \sin \theta_k} \sum_{n=0}^{N-1} \left| y_n - \sum_{k=1}^K x_k e^{-j2\pi \frac{d}{\lambda} n \sin \theta_k} \right|^2$$

This is equivalent to approximating a stream of 1D samples as a finite sum of sinusoids, where the high-accuracy Finite Rate of Innovation (FRI) algorithms can be applied [30], [32]–[34], [42], [44].

ss-FRI DOA Estimation for Single Snapshot. The FRI approximation algorithm is built upon model-fitting [42], [44], [45], [46]. The first key idea is that the Discrete Fourier Transform (DFT) of a sum of K sinusoids can be expressed as ratio of two polynomials in $e^{-j2\pi n/N}$: a numerator polynomial P_{K-1} of degree $K-1$ and a denominator Q_K of degree K

$$\begin{aligned} \hat{y}_n &= \sum_{n'=0}^{N-1} y_{n'} e^{-j \frac{2\pi n' n}{N}} \\ &= \sum_{n'=0}^{N-1} \left(\sum_{k=1}^K x_k e^{-j2\pi \frac{d}{\lambda} n' \sin \theta_k} \right) e^{-j \frac{2\pi n' n}{N}} \\ &= \sum_{k=1}^K x_k \frac{1 - e^{-j(2\pi N \lambda \sin \theta_k)/d}}{1 - z e^{-j(2\pi \lambda \sin \theta_k)/d}} \\ &= \frac{P_{K-1}(z)}{Q_K(z)} \end{aligned} \quad (2)$$

where \hat{y}_n denotes the DFT of the signal y_n and $z = e^{-j2\pi n/N}$. In fact, the denominator polynomial Q_K is the annihilation filter in [31] whose zeros uniquely define the DOAs $\sin \theta_k$ of the signal y_n . This ratio relationship reveals the following important aspects:

- 1) The measured sensor samples are uniquely defined by the coefficients of two polynomials P_{K-1} and Q_K . In other words, the signal can be exactly recovered if these coefficients are known.

- 2) This ratio representation is independent of the number of samples, as the degree of the polynomials is only related to the number of sinusoids.
- 3) It is a sparse representation of the sinusoidal samples.

As a result, this ratio structure is used to perform model-fitting on the DFT of the measured samples in the presence of noise

$$\min_{Q_K, P_{K-1}} \sum_{n=0}^{N-1} \left| \hat{y}_n - \frac{P_{K-1}(z)}{Q_K(z)} \right|^2 \quad (3)$$

The second key idea is to consider that any K -sinusoidal approximation that fits the measured data within a given noise margin is a valid solution. More specifically, the FRI recovery is successful as soon as the criterion

$$\text{MSE}_{\text{rec}} \leq \sigma_{\text{noise}}^2 \quad (4)$$

is satisfied, where MSE_{rec} is the mean square error (MSE) between the reconstructed samples and measurements y_n . σ_{noise}^2 denotes the input noise level, which matches the minimization defined in (3) and can be estimated from measurements (e.g. background noise, instrument inaccuracy, etc.).

The minimization as stated in (3) is non-linear and non-convex. Its direct computation would require non-linear based methods, such as the Newton-Gauss method or the Levenberg-Marquard method. In this paper, the solution is estimated in a linear manner using iterative minimization [42], [47], [48], i.e. solving the following quadratic minimization problem for Q_K^i

$$\min_{Q_K^{(i)}, P_{K-1}^{(i)}} \sum_{n=0}^{N-1} \left| \frac{Q_K^{(i)}(z) \hat{y}_n - P_{K-1}^{(i)}(z)}{Q_K^{(i-1)}(z)} \right|^2 \quad (5)$$

gives rise to a batch of candidates for Q_K ($i = 1, 2, \dots, i_{\text{max}}$), and choose the one for which the MSE is the smallest. Changing the initializations of these iterations provides even more candidates. Usually, two random initializations and $i_{\text{max}} = 20$ are sufficient to attain a solution that is within the expected noise margin. Refer the reader to [30], [42] for more details.

The DOAs $\sin \theta_k$, $k = 1, 2, \dots, K$ can be obtained by computing the zeros of the polynomial ($Q_K(z_k) = 0$)

$$\sin \theta_k = \text{Real} \left(-\frac{\lambda \log(z_k)}{2\pi d} j \right) \quad (6)$$

and the associated coefficients can be acquired by

$$x_k = \left. \frac{(1 - z_k^{-1} z) P_{K-1}(z)}{(1 - z_k^{-N}) Q_K(z)} \right|_{z=z_k} \quad (7)$$

which gives the sparse recovery of the 1D measured sensor samples.

B. Multiple Snapshot ss-FRI DOA Estimation

Signal Model for Multiple Snapshots. Given K stationary sources and L signal snapshots, the DOA estimation in presence of noise can then be formulated as

$$\min_{x_{k,l}, \sin \theta_k} \sum_{l=1}^L \sum_{n=0}^{N-1} \left| y_{n,l} - \sum_{k=1}^K x_{k,l} e^{-j2\pi \frac{d}{\lambda} n \sin \theta_k} \right|^2$$

where $y_{n,l}$ is the measurement of the n -th sensor node in l -th signal collection.

Some multiple-snapshot DOA estimation algorithms rely on the hypothesis of incoherent sources to compute the covariance matrix, which does not match many practical applications, e.g. coherent arrivals caused by multipath in underwater acoustic or speech signal processing. Violation of this hypothesis results into degradation of the rank of the covariance matrix, and thereby large inaccuracies occur in DOA estimation [5]. With ss-FRI algorithm, this incoherence hypothesis is not necessary and the multiple snapshot data helps improve the accuracy and robustness of DOA estimation.

ss-FRI DOA Estimation for Multiple Snapshots. The initial FRI algorithm based on ratio-structure model is essentially designed for single-snapshot uniform sensor data [42]. When dealing with real multiple snapshot data, simply averaging the DOA estimates obtained from each individual signal snapshot is not accurate and robust enough. Hence, a unified FRI model is needed to efficiently process multiple snapshot sensor measurements.

Each individual snapshot of sensor signals can be expressed as

$$\hat{y}_{n,l} = \frac{P_{K-1,l}(z)}{Q_K(z)}, \quad l = 1, 2, \dots, L$$

where the denominator polynomial Q_K is invariant across all signal snapshots due to stationary sources. Following the same fitting principle, the FRI recovery is considered to be successful as soon as the reconstructed signal samples fit the sensor measurements within a given noise margin (see (4)). Hence, similar to minimization (3), the model-fitting performed on the DFT of the multiple-snapshot signal samples can be formulated as

$$\min_{Q_K, P_{K-1,l}} \sum_{l=1}^L \sum_{n=0}^{N-1} \left| \hat{y}_{n,l} - \frac{P_{K-1,l}(z)}{Q_K(z)} \right|^2 \quad (8)$$

where $\hat{y}_{n,l}$ denotes the DFT of the samples $y_{n,l}$. The coefficients of two polynomials $Q_K, P_{K-1,l}$ uniquely define the DOAs $\sin \theta_k$ and coefficients $x_{k,l}$ of the multiple snapshot sensor samples.

Following the linear strategy in (5), Q_k can be obtained by solving the following quadratic minimization problem

$$\min_{Q_K^{(i)}, P_{K-1,l}^{(i)}} \sum_{l=1}^L \sum_{n=0}^{N-1} \left| \frac{Q_K^{(i)}(z) \hat{y}_{n,l} - P_{K-1,l}^{(i)}(z)}{Q_K^{(i-1)}(z)} \right|^2 \quad (9)$$

out of which the candidate with the smallest MSE is chosen. An efficient implementation of this iterative minimization is described in Sec IV-B.

The DOAs $\sin \theta_k$ can be obtained via (6). The ensemble amplitudes $|x_k|$ are the incoherent superposition of each individual snapshot

$$|x_k| = \left(\frac{1}{L} \sum_{l=1}^L |x_{k,l}|^2 \right)^{\frac{1}{2}}, \quad (10)$$

where $x_{k,l}$ is the estimated amplitude of l -th snapshot acquired by (7).

III. SS-FRI DOA ESTIMATION FOR NON-UNIFORM ARRAYS

Uniform sampling is a basic assumption in many high-resolution DOA estimation techniques, whereas it does not always hold in many scenarios. For example, sensor data loss or damage frequently occurs in ocean sound source localization and tracking. In this part, the FRI approximation is further extended to the non-uniform sampling, where only several sensor measurements (random selected) of uniform sensor array are available.

Signal Model for Non-uniform Arrays. When given L multiple snapshots of K stationary sources, consider a ULA with N uniform sensors. After data collection, only a small subset M^2 of N sensor nodes can be used. In such circumstances, the usable sensor samples $\mathbf{Y}_M = [\mathbf{y}_{M,1}, \mathbf{y}_{M,2}, \dots, \mathbf{y}_{M,L}]$, $\mathbf{Y}_M \in \mathbb{C}^{M \times L}$ can be expressed as in matrix form

$$\mathbf{Y}_M = \mathbf{G} \mathbf{Y}_N, \quad M < N$$

where $\mathbf{Y}_N = [\mathbf{y}_{N,1}, \mathbf{y}_{N,2}, \dots, \mathbf{y}_{N,L}]$, $\mathbf{Y}_N \in \mathbb{C}^{N \times L}$ is the uniform sample matrix, $\mathbf{y}_{M,l}$ denotes the usable sensor samples of the l -th snapshot, and $\mathbf{y}_{N,l}$ denotes the uniform samples of the l -th snapshot. The matrix \mathbf{G} is the sub-sampled identity matrix that has exactly one entry of 1 in each row and 0 s elsewhere.

Retrieving DOAs and amplitudes from such non-uniform signal samples is challenging since they are randomly selected from a collection of uniform measurements in presence of strong noise. In order to tackle this problem, the ratio-structure model is further generalized to directly perform model-fitting on the non-uniform samples.

ss-FRI DOA Estimation for Non-uniform Arrays. First, by defining \mathbf{W} as a $N \times N$ inverse DFT matrix, the following is shown

$$\mathbf{y}_{N,l} = \mathbf{W} \left\{ \frac{P_{K-1,l}(z)}{Q_K(z)} \right\}_{n=0}^{N-1}$$

which results from (2) and $z = e^{-j2\pi n/N}$. $\mathbf{W}_{u,v} = \frac{1}{N} \exp(j2\pi uv/N)$. Using this signal representation, the usable sensor samples can be expressed as

$$\mathbf{y}_{M,l} = \mathbf{G} \mathbf{W} \left\{ \frac{P_{K-1,l}(z)}{Q_K(z)} \right\}_{n=0}^{N-1}$$

which effectively provides a non-uniform sample model comprising a ratio of two polynomials that is not far from our FRI approximation framework. Hence, in noisy conditions, the FRI DOA estimation for non-uniform arrays can then be formulated as

$$\min_{Q_K, P_{K-1,l}} \sum_{l=1}^L \left\| \mathbf{y}_{M,l} - \mathbf{G} \mathbf{W} \left\{ \frac{P_{K-1,l}(z)}{Q_K(z)} \right\}_{n=0}^{N-1} \right\|^2 \quad (11)$$

where model-fitting is performed on the signal samples directly instead of the DFT samples.

²To ensure that the total problem is well-posed, i.e. the number of parameters to be retrieved is less than the number of sensors, in practice it is usually required that $M \geq 2K + 1$.

Using the similar strategy as stated in (5), the problem is solved in a linear manner using the following iterative minimization

$$\min_{Q_K^{(i)}, P_{K-1,l}^{(i)}} \sum_{l=1}^L \left\| \mathbf{G}\mathbf{W} \left\{ \frac{Q_K^{(i)}(z)\bar{y}_{n,l} - P_{K-1,l}^{(i)}(z)}{Q_K^{(i-1)}(z)} \right\}_{n=0}^{N-1} \right\|^2$$

$$\text{s.t. } \|\mathbf{Y}_M - \mathbf{G}\mathbf{W}\bar{\mathbf{Y}}_N\|^2 \leq \sigma_{\text{noise}}^2 \quad (12)$$

where $\bar{\mathbf{Y}}_N = \{\bar{y}_{n,l}\}_{n=0, l=1}^{N-1, L}$ is the predicted DFT of the uniform sensor sample matrix \mathbf{Y}_N via the known non-uniform measurements \mathbf{Y}_M . Solving the constrained iterative quadratic minimization problem for $Q_K^{(i)}$ provides a collection of candidates for Q_K , when $i = 1, \dots, i_{\max}$, out of which the one for which the MSE is the smallest is selected. The details of the implementation for (12) in Sec IV.

IV. ALGORITHMIC SETTING

The FRI algorithm based on model-fitting is very robust and efficient that reaches Cram é r-Rao lower bounds (CRLB) empirically for a large range of noise level (SNR ≥ 5 dB) [44]. In this paper, the generic FRI framework is proposed to apply to the multiple snapshot and non-uniform scenes. Applying the MSE criterion, the FRI recovery is considered to be successful as soon as the MSE between the signal reconstruction and the measured samples is within the expected noise margin.

The DOA estimation for the single snapshot signal can be considered as a special case of the multiple snapshot scenarios, which essentially shares the same signal model and fitting principle. Hence, this section focuses on the algorithmic implementation of the FRI approximation for multiple snapshots and non-uniform measurements.

A. Model Order

For the MSE criterion, any sum of K sinusoids that is close enough, i.e. within the given noise margin σ_{noise}^2 , to the measured samples is a valid solution. Therefore, following a parsimony principle, the ‘‘best’’ model order can be determined as the smallest value of K for which this sum of sinusoids is a valid solution. The detailed description of this model-order determination algorithm is presented in [43].

B. ss-FRI DOA Estimation for Multiple Snapshots

Start with rewriting (9) in terms of the product of Fourier matrices. First, by defining $\mathbf{W}_{N,K}^H$ as a $N \times K$ DFT matrix, for l -snapshot samples, it can be expressed as

$$\{P_{K-1,l}(z)\}_{n=0}^{N-1} = \mathbf{W}_{N,K}^H \mathbf{p}_l$$

$$\{Q_K(z)\}_{n=0}^{N-1} = \mathbf{W}_{N,K+1}^H \mathbf{q}$$

where \mathbf{p}_l , \mathbf{q} are the coefficients of polynomials $P_{l,K-1}$, Q_K which uniquely defines the DOA $\sin \theta_k$ and amplitude $x_{k,l}$ of the l -th snapshot signals. Now, define $\hat{\mathbf{y}}_{N,l} = [\hat{y}_{0,l}, \hat{y}_{1,l}, \dots, \hat{y}_{N-1,l}]^T$ as the DFT of the l -th snapshot measurement vector, and $\text{diag}\{\hat{\mathbf{y}}_{N,l}\}$ as the diagonal matrix constructed

from $\hat{\mathbf{y}}_{N,l}$. Then, the quadratic minimization (9) becomes

$$\min_{\tilde{\mathbf{p}}, \mathbf{q}_i} \|\mathbf{A}_{i-1} \mathbf{q}_i - \mathbf{B}_{i-1} \tilde{\mathbf{p}}_i\|^2 \quad (13)$$

where $\tilde{\mathbf{p}} = [\mathbf{p}_1^T, \mathbf{p}_2^T, \dots, \mathbf{p}_L^T]^T$ is numerator polynomial coefficients vector of all snapshots. The matrices \mathbf{A}_{i-1} , \mathbf{B}_{i-1} are given by

$$\mathbf{A}_{i-1} = \begin{bmatrix} \text{diag}\{\hat{\mathbf{y}}_{N,1}\} \\ \text{diag}\{\hat{\mathbf{y}}_{N,2}\} \\ \vdots \\ \text{diag}\{\hat{\mathbf{y}}_{N,L}\} \end{bmatrix} \underbrace{(\text{diag}\{\mathbf{W}_{N,K+1}^H \mathbf{q}_{i-1}\})^{-1} \mathbf{W}_{N,K+1}^H}_{\stackrel{\text{def}}{=} \tilde{\mathbf{R}}_{i-1}}$$

$$\mathbf{B}_{i-1} = \tilde{\mathbf{R}}_{i-1} \tilde{\mathbf{W}}$$

where $\tilde{\mathbf{R}}, \tilde{\mathbf{W}}$ are given by

$$\tilde{\mathbf{R}}_{i-1} \stackrel{\text{def}}{=} \begin{bmatrix} \mathbf{R}_{i-1} & 0 & \cdots & 0 \\ 0 & \mathbf{R}_{i-1} & \cdots & 0 \\ \vdots & \vdots & \ddots & \vdots \\ 0 & 0 & \cdots & \mathbf{R}_{i-1} \end{bmatrix} \in \mathbb{C}^{NL \times NL},$$

$$\tilde{\mathbf{W}} \stackrel{\text{def}}{=} \begin{bmatrix} \mathbf{W}_{N,K}^H & 0 & \cdots & 0 \\ 0 & \mathbf{W}_{N,K}^H & \cdots & 0 \\ \vdots & \vdots & \ddots & \vdots \\ 0 & 0 & \cdots & \mathbf{W}_{N,K}^H \end{bmatrix} \in \mathbb{C}^{NL \times KL} \quad (14)$$

Note that, \mathbf{R}_{i-1} is a square matrix with full rank and $\mathbf{W}_{N,K}^H$ is a $N \times K$ DFT matrix with full column rank, so \mathbf{B}_{i-1} is a matrix with full column rank. A normalization constraint is needed to ensure the uniqueness of the solution \mathbf{q}_i to (9), where $c_0 \mathbf{q}_i$ (c_0 is any arbitrary non-zero constant) is still a valid solution. In this paper, we use the linear unit constraint: $\mathbf{q}_0^H \mathbf{q}_i = 1$, where \mathbf{q}_0 is random initialized. Therefore, with this linear constraint, the minimization in (13) can be rewritten as

$$\min_{\mathbf{q}_i} \left\| (\mathbf{I} - \mathbf{B}_{i-1} \mathbf{B}_{i-1}^\dagger) \mathbf{A}_{i-1} \mathbf{q}_i \right\|^2 \text{ s.t. } \mathbf{q}_0^H \mathbf{q}_i = 1 \quad (15)$$

where $\mathbf{B}_{i-1}^\dagger = [\mathbf{B}_{i-1}^H \mathbf{B}_{i-1}]^{-1} \mathbf{B}_{i-1}^H$. The next iteration \mathbf{q}_i is estimated by solving (15) using total least squares, thus QR decomposition is performed.

For each coefficient initialization \mathbf{q}_0 , we keep iterating the polynomial coefficients \mathbf{q} until the MSE criterion is satisfied. We reinitialize the coefficient \mathbf{q}_0 if the maximum iteration number ($= i_{\max}$) is attained under the same initialization \mathbf{q}_0 . In practice, 5 random coefficient initialization and $i_{\max} = 20$ are sufficient to obtain a solution that is within the expected noise margin. We summarize the main procedure in Algorithm 1.

In practical applications, it is very likely that there are outliers in the multiple snapshot sensor data. Here, we provides a simple way to remove the outliers: find the individual snapshot data from which the estimated DOAs are far from the DOAs using the full multiple snapshot data. With the ‘‘cleaned’’ multiple snapshot data, the accuracy and robustness of DOA estimation can be further improved.

Algorithm 1: Multiple Snapshot ss-FRI DOA Estimation.

Input: Multiple snapshot measurements \mathbf{Y}_N ,
noise level σ_{noise}^2

Output: Denominator polynomial coefficients \mathbf{q} ,
numerator polynomial coefficients $\tilde{\mathbf{p}}$,
the DOAs $\sin \theta_k$,
the amplitudes $|x_k|$

for $loop = 1$ to *max. initializations* **do**
Initialize \mathbf{q} with a random vector \mathbf{q}_0 ;
for $i = 1$ to *max. iterations* **do**
Build the matrices involved in (15) with \mathbf{q}_{i-1} , such as
 \mathbf{A}_{i-1} , \mathbf{B}_{i-1} , and etc;
Update \mathbf{q}_i by solving (15);
if $\sum_{l=1}^L \sum_{n=0}^{N-1} |\hat{y}_{n,l} - \frac{P_{K-1,l}(z)}{Q_k(z)}|^2 \leq \sigma_{\text{noise}}^2$ **then**
Calculate $\tilde{\mathbf{p}}$ by solving (13);
Terminate all loops;
end if
end for
end for
 $\mathbf{q} = \mathbf{q}_i$, $\tilde{\mathbf{p}} = \tilde{\mathbf{p}}$;
Calculate $\sin \theta_k$ and $|x_k|$ using (6), (7) and (10).

Algorithm 2: ss-FRI DOA Estimation for Non-Uniform Arrays.

Input: Multiple snapshot non-uniform measurements \mathbf{Y}_M ,
the rectangular permutation matrix \mathbf{G} , noise level σ_{noise}^2

Output: Denominator polynomial coefficients \mathbf{q} ,
numerator polynomial coefficients $\tilde{\mathbf{p}}$,
the DOAs $\sin \theta_k$,
the amplitudes $|x_k|$

for $loop = 1$ to *max. initializations* **do**
Initialize $\{\tilde{y}_{n,l}\}$ with a random vector $\{\tilde{y}_{n,l}\}_0$;
running Algorithm 1 to obtain \mathbf{q}_0 , $\tilde{\mathbf{p}}_0$ and $\mathbf{Y}_{\text{rec}}^0$;
for $i = 1$ to *max. iterations* **do**
Update $\tilde{\mathbf{Y}}_N$ using (16);
Update \mathbf{q}_i , $\tilde{\mathbf{p}}_i$ and $\mathbf{Y}_{\text{rec}}^i$ by running Algorithm 1;
if $\|\mathbf{Y}_M - \mathbf{G}\mathbf{W}\mathbf{Y}_{\text{rec}}^i\|_F^2 \leq \sigma_{\text{noise}}^2$ **then**
Terminate all loops;
end if
end for
end for
 $\mathbf{q} = \mathbf{q}_i$, $\tilde{\mathbf{p}} = \tilde{\mathbf{p}}_i$;
Calculate $\sin \theta_k$ and $|x_k|$ (6), (7) and (10).

C. ss-FRI DOA Estimation for Non-Uniform Arrays

The new FRI scheme provides a possibility to directly perform model-fitting on the non-uniform sensor measurements \mathbf{Y}_M . Notice that, the sub-sampled identity matrix \mathbf{G} is of full rank, hence the predicted DFT of the uniform samples $\tilde{\mathbf{Y}}_N$ cannot be uniquely determined via the constrains in (12).

Applying a model-fitting principle, the key idea is that the correct predicted DFT samples $\tilde{\mathbf{Y}}_N$ best fit the ratio-structure model. In other words, given a collection of candidates for $\tilde{\mathbf{Y}}_N$, the correct DFT samples should be the one for which the MSE is the smallest. This provides an efficient way to estimate the solution to (11) in a linear manner by alternatively optimizing DFT samples and polynomial coefficients:

- 1) Given DFT samples $\tilde{\mathbf{Y}}_N$, Update polynomial coefficients $P_{K-1,l}^{(i)}$, $Q_K^{(i)}$ by applying the FRI algorithm.
- 2) Recover the FRI DFT signal \mathbf{Y}_{rec} based on the ratio-structure model.
- 3) Update DFT samples $\tilde{\mathbf{Y}}_N$ by

$$\min_{\tilde{\mathbf{Y}}_N} \|\tilde{\mathbf{Y}}_N - \mathbf{Y}_{\text{rec}}\|_F^2, \text{ s.t. } \|\mathbf{Y}_M - \mathbf{G}\mathbf{W}\tilde{\mathbf{Y}}_N\|_F^2 \leq \sigma_{\text{noise}}^2 \quad (16)$$

where the subscript F represents the Frobenius norm.

It is straightforward to see that, geometrically (16) is equivalent to the orthogonal projection of the recovered FRI DFT signal \mathbf{Y}_{rec} to the M -dimensional sphere: $\|\mathbf{Y}_M - \mathbf{G}\mathbf{W}\tilde{\mathbf{Y}}_N\|_F^2 \leq \sigma_{\text{noise}}^2$, i.e. the proximal mapping of the signal recovery \mathbf{Y}_{rec} .

Hence, by repeating these steps, the model-fitting error as stated in (12) would fast decrease, where it stops as soon as the criteria (4) is satisfied. The initialization of the DFT samples $\tilde{\mathbf{Y}}_N$ is randomly selected in the solution space, i.e. $\tilde{\mathbf{Y}}_N \in \{\mathbf{Y}_M - \mathbf{G}\mathbf{W}\tilde{\mathbf{Y}}_N\|_F^2 \leq \sigma_{\text{noise}}^2\}$. Typically, ten random initializations and $i_{\text{max}} = 20$ are sufficient to obtain a solution to the problem that

is within the expected noise margin. The detailed algorithmic implementation is described in Algorithm 2.

In fact, the FRI DOA estimation technique for the ULAs can be seen as a special case of the non-uniform array, because we have $\mathbf{G}^T \mathbf{G} = \mathbf{I}_d$ (\mathbf{I}_d represents the identity matrix). That is, this paper proposes a unified FRI algorithm based on ratio-structure model, i.e. Algorithm 2, to solve the most common DOA estimation problem in practice, such as single snapshot with uniform samples, multiple snapshots with uniform samples, single snapshot with non-uniform samples, multiple snapshots with non-uniform samples. With high-resolution and low computational cost, our ss-FRI algorithm can robustly tackle a wide variety of DOA-related tasks in practice.

D. Algorithmic Complexity

In terms of computational cost, the model-fitting method requires the QR decomposition of matrix \mathbf{A}_{i-1} and \mathbf{B}_{i-1} . It seems that in each inner iteration, our method requires a QR decomposition of the matrix $\mathbf{A}_{i-1} \in \mathbb{C}^{NL \times (K+1)}$ and the matrix $\mathbf{B}_{i-1} \in \mathbb{C}^{NL \times KL}$. However, the square matrix \mathbf{B}_{i-1} is repetitive along the diagonal.

$$\mathbf{B}_{i-1}^\dagger = \begin{bmatrix} (\mathbf{C}_{i-1})^{-1} & 0 & \cdots & 0 \\ 0 & (\mathbf{C}_{i-1})^{-1} & \cdots & 0 \\ \vdots & \vdots & \ddots & \vdots \\ 0 & 0 & \cdots & (\mathbf{C}_{i-1})^{-1} \end{bmatrix} \mathbf{B}_{i-1}^H \quad (17)$$

where $\mathbf{C}_{i-1} = (\mathbf{R}_{i-1} \mathbf{W}_{N,K}^H)^H \mathbf{R}_{i-1} \mathbf{W}_{N,K}^H$ and it essentially only needs to perform a QR decomposition on a K -square matrix \mathbf{C}_{i-1} . Moreover, notice that, the matrix \mathbf{B}_{i-1} is also sparse whose algebraic structure largely reduces the matrix building and computational cost. Hence, the computational complexity mainly scales with the number of sources K and varies slowly

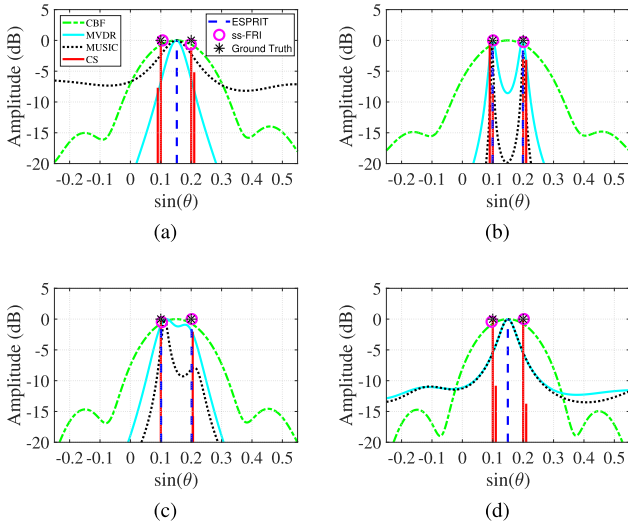


Fig. 2. DOA estimation from L snapshots for two equal strength sources (*) at 0.1 and 0.2 with SNR = 20 dB. CBF, MVDR, MUSIC, CS, ESPRIT and ss-FRI DOA estimation for incoherent sources with (a) $L = 1$, (b) $L = 64$, and (c) $L = 3$, and (d) for coherent sources with $L = 64$. The ULA has 10 sensors.

with the number of samples and snapshots, which significantly increases the algorithm run-speed when processing real DOA data (e.g. many sensors and snapshots).

V. SIMULATION RESULTS

In this section, the proposed ss-FRI DOA estimation algorithm is validated in various conditions. In the first part, the performance comparison between our algorithm and other high-resolution techniques is concretely presented in Section V-A. Then, the dependence of the DOA estimation performance on possible parameters (e.g. position perturbations of sensors, number of data snapshots, SNR, etc.) is thoroughly investigated in Section V-B.

To perform these simulations, the algorithm is implemented in MATLAB 2019b on a computer with i7 – 7700 CPU and 16 G of RAM. The divided grid of CBF, MVDR, MUSIC, and CS is set as $[-1 : 0.01 : 1]$ by default. The element spacing (i.e. sensor interval) of all ULAs is half a wavelength, which gives rise to: $\frac{d}{\lambda} = 0.5$. For non-uniform arrays, the minimum spacing of the array elements is also half a wavelength. The CVX (convex) toolbox is used to implement Compressive Sensing techniques in the MATLAB environment, and we refer the readers to [5] for more details.

A. Performance Comparison

In this section, ss-FRI is compared with commonly used algorithms such as CBF, MVDR, MUSIC, ESPRIT, and CS in several aspects: resolution, weak target detection for uniform and non-uniform arrays, and basis mismatch.

1) *Resolution*: Resolution of DOA estimation is very important in many practical applications, which directly determines the performance of the DOA-related tasks. Fig. 2(a) shows the estimation resolution of ss-FRI, CBF, MVDR, MUSIC, ESPRIT, and CS under the condition of single snapshot and incoherent

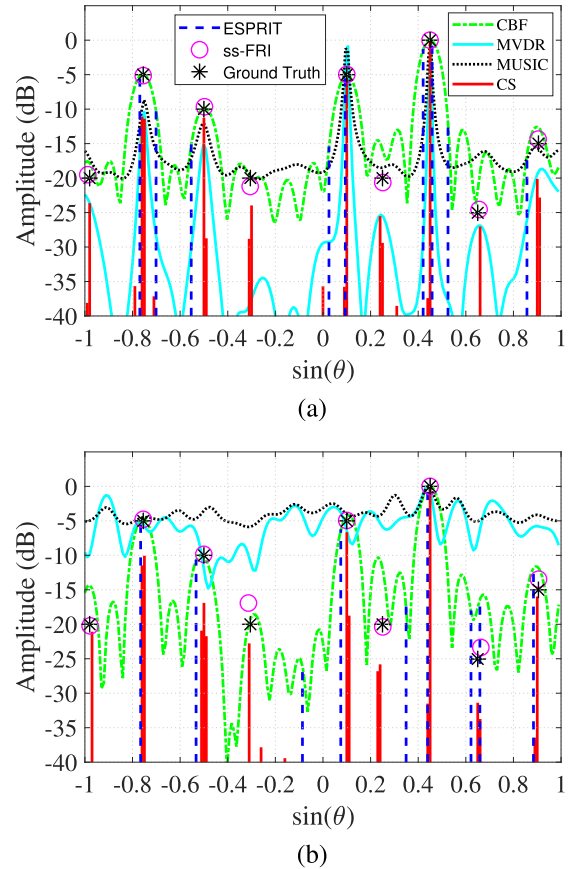


Fig. 3. Multiple snapshot ($L = 5$) DOA estimation for nine sources (*) at $-0.98, -0.755, -0.5, -0.305, 0.1, 0.25, 0.45, 0.65,$ and 0.905 with SNR = 0 dB, 15 dB, 10 dB, 0 dB, 15 dB, 0 dB, 20 dB, -5 dB, and 5 dB, respectively. CBF, MVDR, MUSIC, CS, ESPRIT and ss-FRI DOA estimation for (a) incoherent sources and (b) coherent sources. The ULA has 21 sensors.

sources. Here, the two sources with the same strength (SNR = 20 dB) are located at 0.1 and 0.2. The ULA has 10 sensors. MVDR, MUSIC, and ESPRIT cannot resolve the two sources because of insufficient data snapshots. Fig. 2(b)–(d) show the results of multiple snapshot DOA estimation in incoherent sources and coherent sources cases. CBF fails to discriminate the two closely located sources in all cases. MVDR, MUSIC, and ESPRIT retrieve the incoherent sources successfully, whereas their performance degrades significantly as the number of snapshots decreases.

Notice that, these methods are not robust enough to discriminate the coherent sources due to the degradation of the rank of the covariance matrix. CS is able to resolve the coherent sources, despite the drawbacks of false targets due to spectrum leakage. From Fig. 2, it can be seen that our ss-FRI algorithm is very robust that can accurately retrieve the source locations in various conditions.

2) *Weak Target Detection for ULAs*: Weak target detection is a challenging problem in practice due to the presence of strong interferences and inadequate data snapshots. Fig. 3(a) and (b) present the results of DOA estimation with $L = 5$ snapshots in incoherent and coherent source situations respectively. The ULA has 21 sensors. CBF, MVDR, MUSIC, and ESPRIT can recover

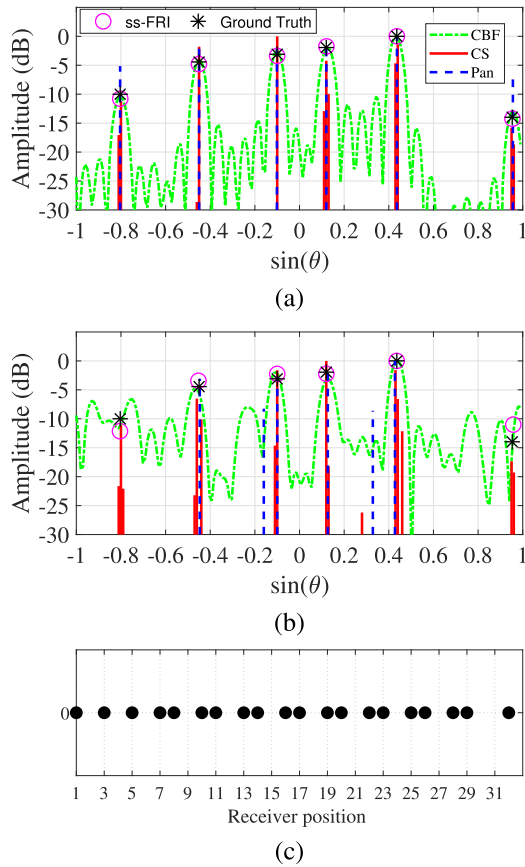


Fig. 4. Single snapshot DOA estimation for uniform and non-uniform array. The sources (*) are at -0.8033 , -0.45 , -0.1 , 0.12 , 0.436 and 0.953 with SNR = 10 dB, 15.5 dB, 17 dB, 18 dB, 20 dB, and 6 dB, respectively. Reconstruction of incoherent sources using CBF, Pan's method, CS and ss-FRI DOA estimation (a) for the ULA (b) and for the non-uniform array. (c) The non-uniform array constructed by randomly selecting $M = 20$ sensors out of a standard ULA with 32 sensors.

the sources with strong strength but fail to locate weak sources in incoherent source case.

When the sources are coherent, they are not able to be applied because of the degradation of the covariance matrix computed (e.g. MVDR, MUSIC, and ESPRIT). Although CS algorithm has obvious responses at the source positions, there are also non-trivial amplitudes nearby that gives rise to less sparse DOA estimates and inaccurate amplitude estimation. As a result of K -sinusoidal approximation, our algorithm provides an exactly K -sparsity DOA estimation that retrieves both the DOAs and the associated amplitudes accurately.

3) *Weak Target Detection for Non-Uniform Arrays*: Fig. 4 depicts the estimation results of CBF, CS, Pan's method (generalized FRI [30]), and ss-FRI DOA estimation for single snapshot. The ULA has 32 sensors and the non-uniform array has 20 usable sensors (see in Fig. 4(c)). CS and ss-FRI achieve good performance in both uniform and non-uniform scenarios. While, CBF cannot distinguish some sources due to the interference of high sidelobes. Pan's method can locate all sources with high accuracy for the ULA.

However, given the non-uniform measurements, Pan's method can only identify a limited range of DOAs, i.e.

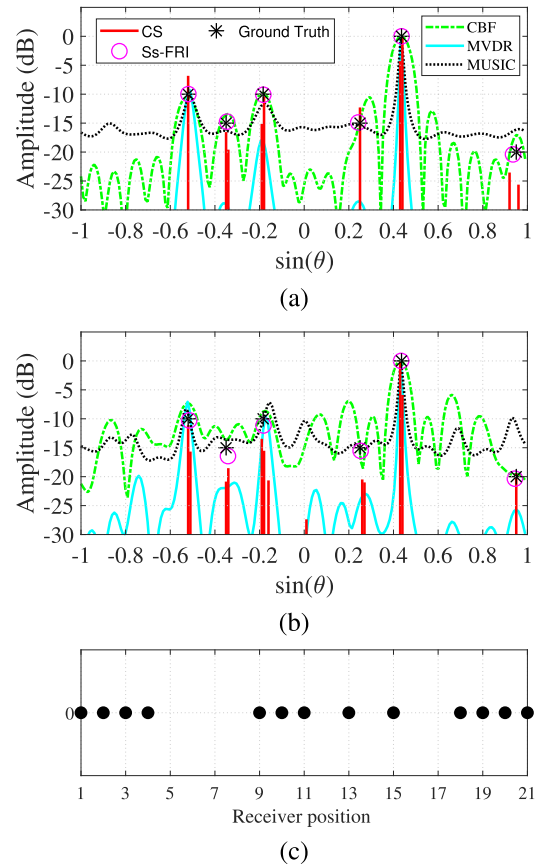


Fig. 5. Multiple snapshot ($L = 3$) DOA estimation for uniform array and non-uniform array. The six sources (*) are at -0.52 , -0.35 , -0.184 , 0.25 , 0.436 and 0.95 with SNR = 10 dB, 5 dB, 10 dB, 5 dB, 20 dB, and 0 dB, respectively. Reconstruction of incoherent sources using CBF, MVDR, MUSIC, CS and ss-FRI DOA estimation (a) for the ULA (b) and for non-uniform array. (c) The non-uniform array constructed by randomly selecting $M = 13$ sensors out of a standard ULA with 21 sensors.

$|\sin(\theta_k)| \leq 0.5$. This is because the minimum spacing of the array elements is half a wavelength that is the most common setting in practice, yet Pan's approach requires the non-uniform measurements to be sufficiently dense in space. As a result, the interval of the interpolated uniform samples by Pan's method is essentially larger than the actual physical distance (half of wavelength), leading to insufficient spatial sampling rate $\frac{d}{\lambda} > 0.5$ [49], [50]. Hence, although Pan's approach is sufficiently robust and accurate to handle arbitrary non-uniform sampling, it is less applicable for the practical DOA applications that make use of the sub-sampled sensor arrays.

For multiple snapshots, there are two cases: one is fixed sources; the other is moving sources. For the fixed sources, the results of uniform and non-uniform arrays with $L = 3$ snapshots are shown in Fig. 5(a) and (b). Fig. 5(c) shows the position of the sensors of the non-uniform array which is constructed by randomly choosing 13 sensors from a ULA comprising of 21 sensors. CBF, MVDR, and MUSIC can all successfully locate the strong sources for the ULA, whereas the non-uniform sampling causes estimation inaccuracy. Consistent with the previous analysis, CS has responses at the ground-truth source positions with less sparse retrieval due to energy leakage. Performing

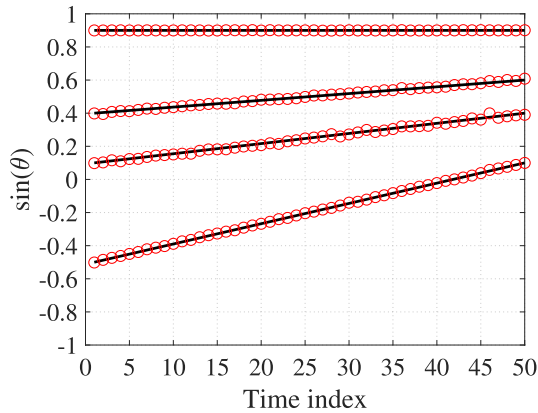


Fig. 6. ss-FRI DOA estimation (\circ) with snapshots ($L = 3$) for four moving sources (solid line) with different SNR = 10 dB, 0 dB, 5 dB and 20 dB (in order of DOAs from small to large) respectively for non-uniform array (the array is the same as Fig. 5(c)).

model-fitting on the non-uniform samples directly, our ss-FRI algorithm accurately recover the DOAs and amplitudes with exactly K -sparsity.

In order to further demonstrate the effectiveness of our algorithm, the test comprising of four moving sources is conducted in the second scenario. The first source moves from -0.5 to 0 with SNR = 10 dB; The second source moves from 0.1 to 0.4 with SNR = 0 dB; The third source moves from 0.4 to 0.6 with SNR = 5 dB; The fourth source is at 0.9 with SNR = 20 dB. The sensor positions are exactly the same as Fig. 5(c). As shown in Fig. 6, the results of ss-FRI accurately coincide with the ground-truth trajectory, which further validates our algorithm in practical settings.

4) *Basis Mismatch*: CS has a pretty good performance in above cases, but it suffers from basis mismatch due to inadequate grid discretization. The fundamental assumption for CS is that the signal can be sparsely represented on the grid, but very likely the target is not exactly located on the grid in practical applications. Consequently, basis mismatch occurs frequently. Fig. 7(a) and (b) show the results of CS without basis mismatch and with basis mismatch respectively. In this circumstances, the ULA has 10 sensors. CS has an extra wrong target detection induced by basis mismatch. Usually, it can be improved by using a denser grid, however, this will lead to the worse orthogonality condition of the sensing matrix built. Besides, this also comes with significant increase on the algorithm computational cost, which is time consuming and prohibited in practice. Using a grid-free ratio-structure model, our algorithm can achieve accurate DOA estimations within a very short run-time.

B. Performance Analysis

In this section, the performance of our ss-FRI algorithm is investigated on the following aspects: sensitivity to sensor position perturbations, multiple-snapshot enhancement, performance curve, and computational time.

1) *Sensitivity to Position Perturbations*: In DOA estimation, the signal model often assumes that the positions of sensors are accurate. However, this assumption usually does not hold in

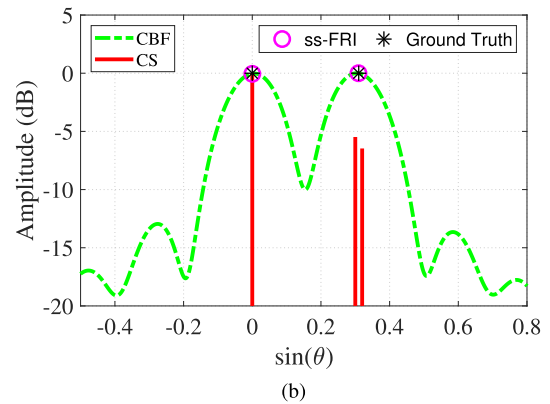
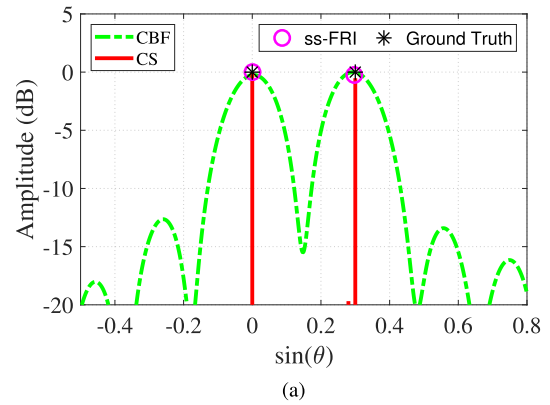


Fig. 7. Single snapshot CS performance in DOA estimation in terms of the discretization of the DOA space. CBF, CS and ss-FRI reconstruction for two equal strength incoherent sources at 0 and 0.31 with SNR = 20 dB. CBF and CS are (a) on a grid $[-1 : 0.01 : 1]$, and (b) on a grid $[-1 : 0.02 : 1]$. The ULA has 10 sensors.

practice, e.g. the turbulent current or the mobile sampling would inevitably influence the sensor displacement. This inaccuracy of sensor positions brings about a series of model degradation, like wide beamwidth, strong sidelobes and disappearance of spectrum peaks [51]. Consequently, it is necessary to check the robustness of our ss-FRI algorithm against the sensor position perturbation.

Fig. 8(b) shows the configuration of the ULA (21 sensors) with large position perturbations that are randomly generated with the standard deviation as 15% of the element spacing (e.g. 0.56 m if $d = 3.75$ m) along both the array direction and vertical direction. Fig. 8(a) shows the results of 60 random realizations for CBF and ss-FRI algorithm, which intuitively demonstrates the robustness of our algorithm against sensor position perturbations.

2) *Multiple Snapshot Enhancement*: The enhancement of running our ss-FRI algorithm with multiple snapshot data is investigated in this part. Fig. 9 intuitively describes the comparison between multiple snapshots and single snapshot. Two sources with the same strength locate at -0.1 and 0.1 with SNR = 0 dB, where the ULA consists of 10 sensors. The ss-FRI with single snapshot gives less accurate estimated DOAs as shown in Fig. 9(a). In this circumstance, the DOA retrieval is intrinsically limited where its estimation inaccuracy can be

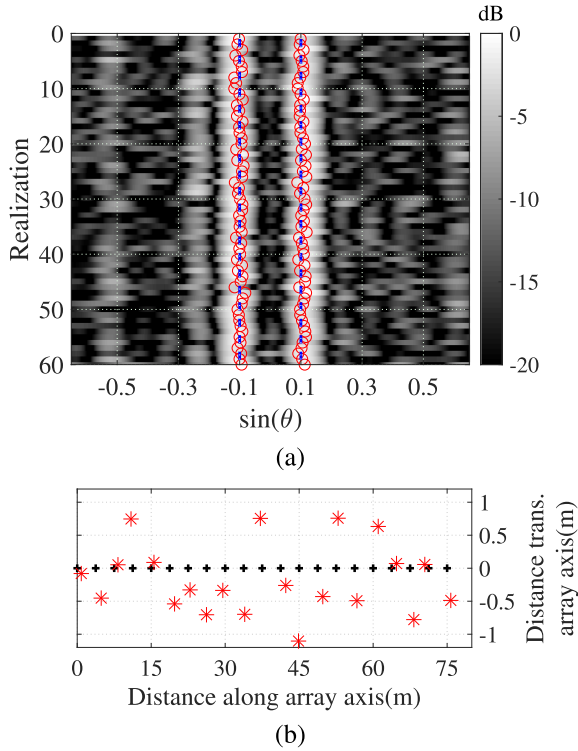


Fig. 8. Single snapshot DOA estimation of two equal strength sources (at 0.1 and -0.1 with $\text{SNR} = 5$ dB) for 60 realizations with position error. (a) Reconstruction with CBF (background color), ss-FRI DOA estimation (\circ) and the true DOAs (the blue vertical dotted line). (b) Top view of the array configuration with position error (“*”) and no position error (“+”). The ULA has 21 sensors.

predicted by computing the Cramér-Rao bounds of the parametric estimation problem [31], [44].

Fig. 9(b) shows the result of CBF and our ss-FRI algorithm under multiple snapshots. Given more available data, the DOA estimation can be significantly improved both on accuracy and robustness. We further use the root mean square error (RMSE) as the evaluation metric to test the ss-FRI algorithm

$$\text{RMSE} = \sqrt{\mathcal{E} \left(\frac{1}{K} \sum_{k=1}^K (\sin \theta_k - \sin \hat{\theta}_k)^2 \right)} \quad (18)$$

where $\sin \hat{\theta}_k$ is the estimated DOA and \mathcal{E} denotes the expected value operator.

Fig. 10(a) shows the relationship between $\text{RMSE} (K = 1)$ and the number of snapshots at different noise level: $\text{SNR} = 0$ dB, 3 dB and 6 dB. The number of snapshots increases from 1 to 100. RMSE decreases rapidly as the number of snapshots increases.

Notice that, the degree of source separation also affects the accuracy of DOA estimation. As shown in Fig. 10(b), RMSE decreases with the increase of source separation and the number of snapshot. The separation of two sources increases from $0.02 \text{ rad}/\pi$ to $0.16 \text{ rad}/\pi$, where SNR increases from 1 dB to 12 dB (the ULA comprises of 10 sensors). In fact, the more separated the sources, the more accurate the final DOA retrieval.

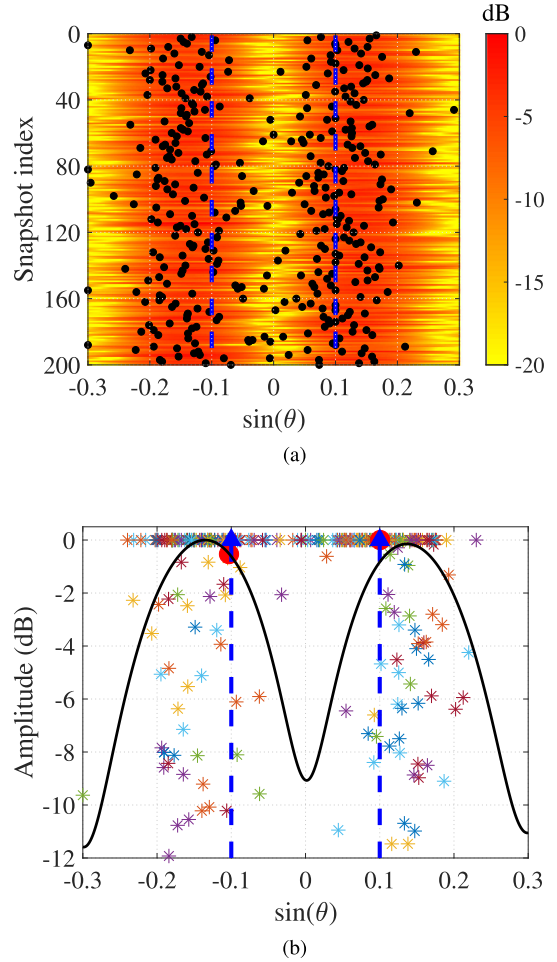


Fig. 9. Comparison of single snapshot and multiple snapshot DOA estimation for two equal strength coherent sources (at 0.1 and -0.1 with $\text{SNR} = 0$ dB, blue vertical dotted lines) along 200 snapshots. (a) Single snapshot CBF (background color) and ss-FRI DOA estimation (dots). (b) Magnitude distribution of single snapshot ss-FRI DOA estimation (*), multiple snapshot ss-FRI DOA estimation (\circ) and ground truth (arrow). The ULA has 10 sensors.

3) *Performance Curve*: In this section, the RMSEs of our ss-FRI algorithm and other methods are compared with the Cramér-Rao lower bounds (CRLB). Fig. 11(a) shows the RMSEs and CRLB with single-snapshot. The ULA consists of 11 sensors and two incoherent sources are located at -0.205 and 0.505 . CS, Cadzow and ss-FRI have a similar performance at low SNR (< 3 dB). However, when signal is less noisy (≥ 3 dB), ss-FRI has a better performance than both CS and Cadzow. Moreover, the computed MSE curve of our ss-FRI algorithm coincides with CRLB at about $\text{SNR} = 4$ dB, which effectively demonstrates its good performance. Note that, CS is limited by grid accuracy at higher SNR.

The results of multiple snapshots ($L = 10$) are shown in Fig. 11(b). Our algorithm outperforms the other techniques. The performance curve of ss-FRI approach reaches the CRLB at -4 dB. Multiple snapshots not only reduce the estimation error, but also make the algorithm reach the CRLB earlier at lower SNR. Therefore, multiple snapshot data provides a DOA estimation with higher robustness and accuracy. Note that, the

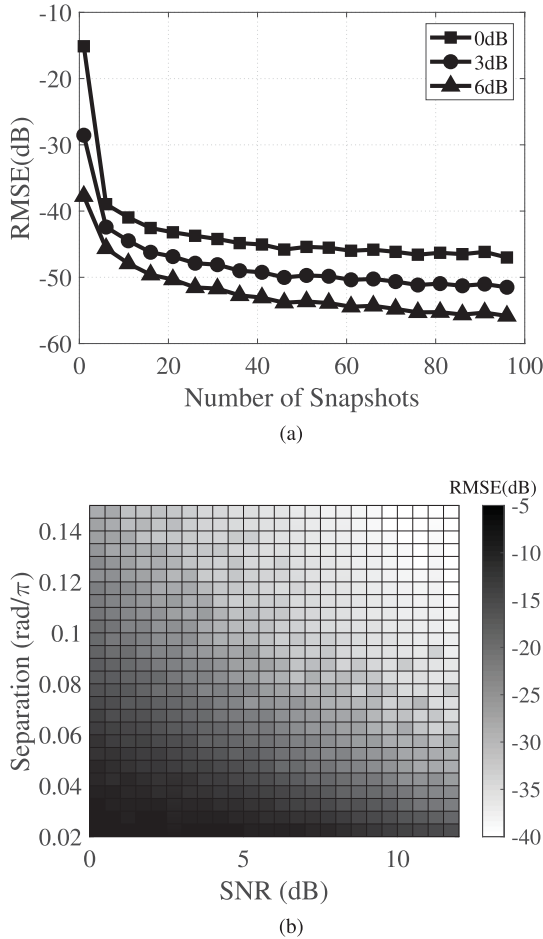


Fig. 10. (a) RMSE (averages over 1000 realizations) for multiple snapshot ss-FRI DOA estimation ($K = 1$) versus number of snapshots with SNR = 0 dB, 3 dB, and 6 dB. (b) RMSE (averages over 1000 realizations) for multiple snapshot ss-FRI DOA estimation versus SNR and Separation between two equal strength incoherent sources with $L = 5$. Note that the ULA has 10 sensors.

curves of MVDR, MUSIC, and CS drift away from the CRLB at higher SNR due to insufficient grid division.

4) *Computation Time*: In this section, we compare the effects of the number of snapshots ($L = 1 : 3 : 31$) and array element number $N = 31 : 30 : 301$ on computation time for CS and ss-FRI. CS is on a grid division as $[-1 : 0.01 : 1]$, which is a commonly used grid accuracy, although it needs to be denser in some scenarios. There are two sources with SNR = 15 dB. The computation times ($L = 1$) of the three methods are shown in Fig. 12(a). The times of both Cadzow and CS increases with the number of sensors N , while the time of ss-FRI (about ≤ 0.01 s) is almost unchanged. ss-FRI only requires a QR decomposition of a small matrix. As shown in Fig. 12(b), the cost of CS also increases with the number of snapshots, whereas ss-FRI rarely varies with the number of snapshots L . This is because the computation of ss-FRI with multiple snapshots can be decoupled as if it was dealing with single-snapshot. Thus, the complexity of our algorithm is mainly related to the number of sources and varies quite slowly with the number of samples and snapshots, which makes it possible to process a large amount of real DOA data within a very short time. This is particularly meaningful

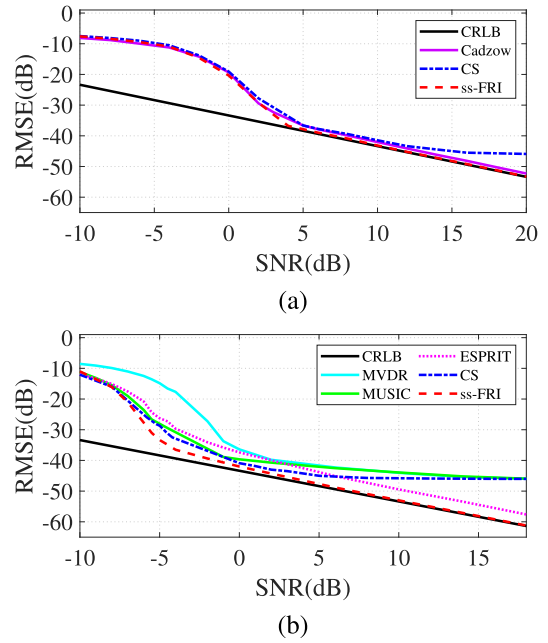


Fig. 11. Comparing the performance curve (averages over 2000 realizations) of Cadzow, MVDR, MUSIC, CS, ESPRIT and ss-FRI DOA estimation with CRLB. There are two equal strength incoherent sources at -0.205 and 0.505 with (a) $L = 1$ and (b) $L = 10$. The ULA has 11 sensors.

for real-time tracking and localization. Fig. 12(c) presents the convergence rate of Cadzow and ss-FRI with 21 sensors, which suggests that less iterations are needed when running our ss-FRI algorithm.

VI. EXPERIMENTAL DATA RESULTS

A. *SWellEx-96 Experiment*

The performance of our ss-FRI algorithm under both single and multiple-snapshots is further validated using real data of a complex multipath shallow-water environment. The data set is from the shallow water evaluation cell experiment 1996 (SWellEx-96) Event S5, occurred from 23:15 to 0:30 in the west of Point Loma, CA.

During the event, the data is collected by a vertical ULA. The array has 64 sensors with spacing $d = 1.875$ m and is distributed from depth 94.125 m to depth 212.25 m. The water depth is 216.5 m. Starting with the first sensor, select one for every three sensors uniformly, the element spacing is thereby $d = 5.625$ m. In addition, the data of the 43 rd sensor is missing, and therefore, the data used is only from non-uniform 21-sensor array. The data of interest occurred at about 00:15 when the depth of the towed source is at depth 54 m and the distance from the array is around 900 m. The towed source signal emitted a set of nine frequencies [112 130,148 166,201 235,283 338,388] Hz. The signal with 112 Hz is used here. The duration data of 1.5 min sampled with 1500 Hz was divided into 87 snapshots of 2.7 s duration with 63% overlap.

Fig. 13(a) shows CBF and ss-FRI DOA estimation for experimental data using the frequency 112 Hz with single snapshot. CBF merges some of the closely located DOAs, while ss-FRI

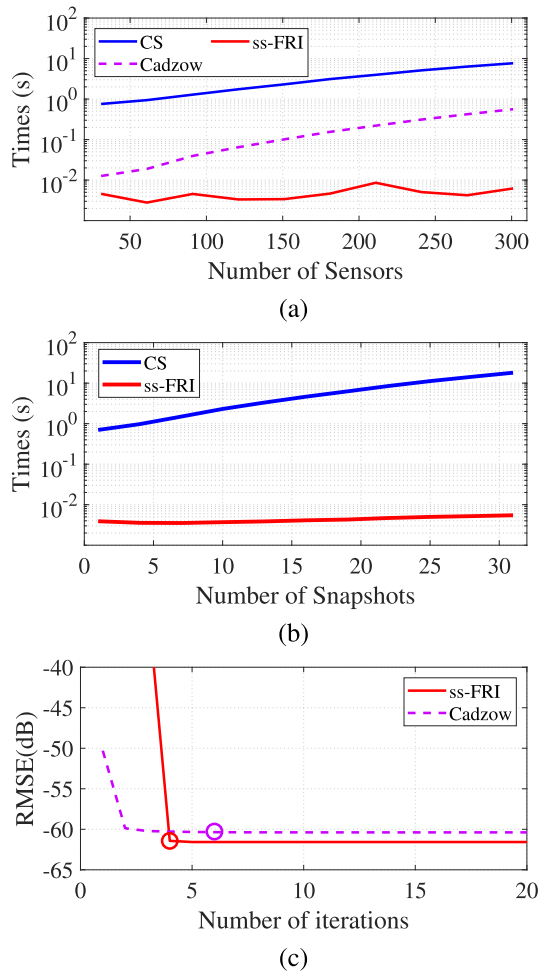


Fig. 12. Comparison of computation time (averages over 500 realizations) for two equal strength incoherent sources with SNR = 15 dB between CS and ss-FRI with (a) different number of sensors N ($L = 1$) and (b) different number of snapshots L ($N = 21$). (c) Convergence rate (averages over 2000 realizations) of Cadzow and ss-FRI for two equal strength sources with SNR = 20 dB and 21 sensors. “o” represents the number of iterations to terminate the loop.

achieves a much better result with higher resolution and sufficient sparsity. More importantly, there are several stationary DOAs along the several snapshots, which may correspond to multipath arrivals in the underwater surroundings. The results of multiple snapshot CBF, MVDR, MUSIC, CS, and ss-FRI DOA estimation are shown in Fig. 13(b). Consistent with the above description, MVDR and MUSIC have unsatisfactory performance even though there are sufficient snapshots data $L = 87$. This is because the data contains the information of the coherent sources due to multipath propagation. CBF cannot distinguish the adjacent paths due to wide mainlobe and high sidelobes. CS and ss-FRI can clearly distinguish the paths submerged by CBF sidelobes. However, CS has a DOA spectrum leakage caused by basis mismatch, which leads to less sparse DOA estimations. Compared with single-snapshot results, there is no significant difference except for some DOAs with very weak energy, because the SNR of most snapshot data is large enough.

Through the comparison of multiple snapshots and single snapshot, the final DOA estimation results are proved to be

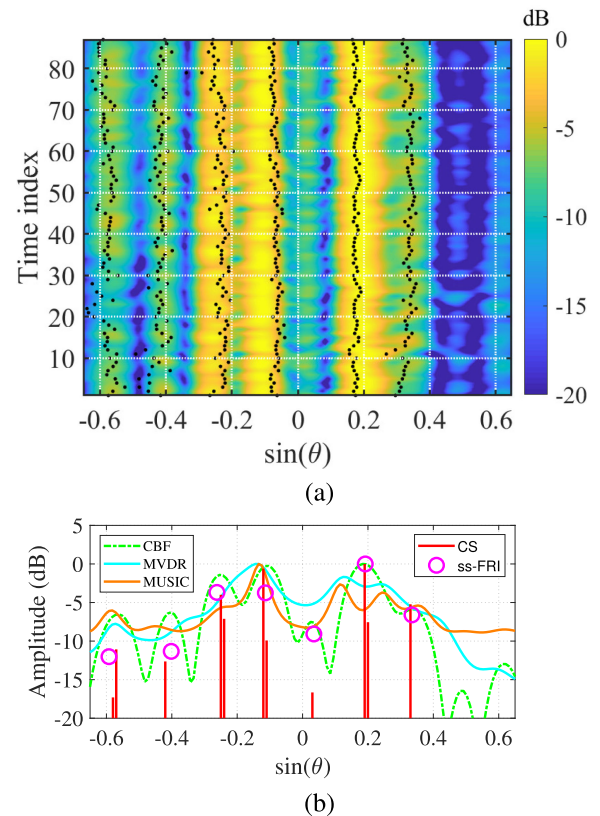


Fig. 13. (a) Single snapshot CBF (background color) and ss-FRI (dots) DOA estimation for frequency $f = 112$ Hz. (b) Multiple snapshot CBF, MVDR, MUSIC, CS, and ss-FRI DOA estimation for frequency $f = 112$ Hz.

sufficiently accurate in some sense (In fact, it is difficult to directly connect DOAs to some very specific paths because the sound speed varies largely with regard to the depth of water, thus virtually the sound does not travel in a way like straight line.).

B. South China Sea Experiment

The second test data was collected by the horizontal towed line array at the South China Sea from August 7 to August 10, 2020. The array has 96 uniform sensors with sampling interval $d = 0.4167$ m (design frequency: 1800 Hz). The data (55 arrival signals) of interest was collected from 23:30, August 7 to 00:40, August 8 when the source remains stationary and the towed array was moving at the depth of 56 m. During this period, the linear frequency modulation (LFM) signal is transmitted in the frequency range of 1700 Hz to 1900 Hz with a duration of 1 s and the period of 50 s. Here, the real DOA trajectory can be obtained from GPS and the attitude sensor data.

Fig. 14(a) demonstrates that ss-FRI DOA estimation for a single snapshot can locate the source correctly, even though the source is moving. In order to further verify the ss-FRI DOA estimation for non-uniform arrays, 12 sensors are randomly selected from 96 sensors. In this case, the sidelobes of CBF increases and appears ambiguity due to non-uniform sampling as shown in Fig. 14(b). Note that, the shape of the towed array is affected by the ocean current and gravity. In general, this will result in the perturbations of sensor positions, which

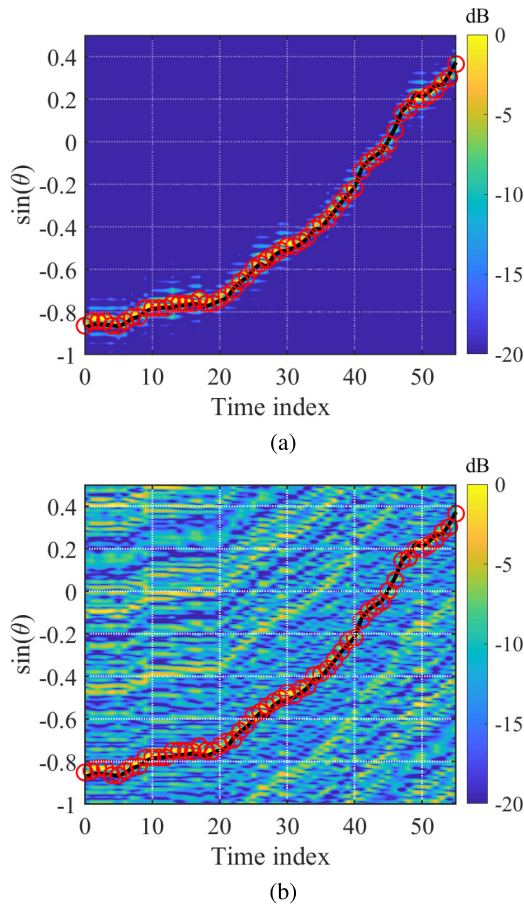


Fig. 14. DOA trajectory estimation (frequency $f = 1800$ Hz) for CBF (background color), ss-FRI (\circ), and GPS (solid line). (a) ULA. (b) Non-uniform array. Note that the non-uniform array constructed by randomly selecting $M = 12$ sensors out of a standard ULA with 96 sensors.

largely deteriorates the DOA estimation. Despite the weak signal strength of sources and this perturbations of sensor positions, our ss-FRI still achieves a sufficiently good recovery within a very short time, which effectively demonstrates the performance of our algorithm when processing real DOA data.

VII. CONCLUSION

Motivated by the practical requirements of various DOA-related tasks, a robust generic DOA estimation method has been proposed in this paper that aims at tackling the common DOA estimation problems (i.e. non-uniform sampling with multiple snapshots) within a short time. Representing the DOA samples as fraction of two polynomials, the model-fitting is directly performed on the non-uniform and multiple snapshot sensor measurements, which leads to a very efficient and robust DOA estimation (ss-FRI) algorithm. We have demonstrated the versatility of the proposed approach via simulated and experimental data in various conditions, e.g. multiple coherent sources, insufficient data snapshots, low SNR, etc. The computational complexity of our algorithm has been proven to be only related to the number of sources independent of both the number of sensors and snapshots, which meets the needs of many DOA-related applications. For future work, the ss-FRI can also be applied

to point source reconstruction in other scenarios. Besides, the ss-FRI DOA estimation for wide-band signals needs more study.

REFERENCES

- [1] J. Capon, "High-resolution frequency-wavenumber spectrum analysis," *Proc. IEEE*, vol. 57, no. 8, pp. 1408–1418, Aug. 1969.
- [2] H. L. V. Trees, *Detection, Estimation, and Modulation Theory, Optimum Array Processing*. New York, NY, USA: Wiley, 2002.
- [3] R. Schmidt, "Multiple emitter location and signal parameter estimation," *IEEE Trans. Antennas Propag.*, vol. AP-34, no. 3, pp. 276–280, Mar. 1986.
- [4] N. Yuen and B. Friedlander, "Asymptotic performance analysis of ESPRIT, higher order ESPRIT, and virtual ESPRIT algorithms," *IEEE Trans. Signal Process.*, vol. 44, no. 10, pp. 2537–2550, Oct. 1996.
- [5] A. Xenaki, P. Gerstoft, and K. Mosegaard, "Compressive beamforming," *J. Acoustical Soc. Amer.*, vol. 136, no. 1, pp. 260–271, 2014.
- [6] D. Malioutov, M. Cetin, and A. S. Willsky, "A sparse signal reconstruction perspective for source localization with sensor arrays," *IEEE Trans. Signal Process.*, vol. 53, no. 8, pp. 3010–3022, Aug. 2005.
- [7] Y. Park, Y. Choo, and W. Seong, "Multiple snapshot grid free compressive beamforming," *J. Acoustical Soc. Amer.*, vol. 143, no. 6, pp. 3849–3859, 2018.
- [8] A. Xenaki and P. Gerstoft, "Grid-free compressive beamforming," *J. Acoustical Soc. Amer.*, vol. 137, no. 4, pp. 1923–1935, 2015.
- [9] Z. Yang and L. Xie, "Enhancing sparsity and resolution via reweighted atomic norm minimization," *IEEE Trans. Signal Process.*, vol. 64, no. 4, pp. 995–1006, Feb. 2015.
- [10] Z. Yang, "Direction-of-arrival estimation using atomic norm methods: Affects of multiple snapshots and coherent sources," in *Proc. IEEE Int. Conf. Comput. Electromagn.*, 2018, pp. 1–3.
- [11] F.-M. Han and X.-D. Zhang, "An ESPRIT-like algorithm for coherent DOA estimation," *IEEE Antennas Wireless Propag. Lett.*, vol. 4, pp. 443–446, 2005.
- [12] T. B. Lavate, V. Kokate, and A. Sapkal, "Performance analysis of MUSIC and ESPRIT DOA estimation algorithms for adaptive array smart antenna in mobile communication," in *Proc. 2nd Int. Conf. Comput. Netw. Technol.*, 2010, pp. 308–311.
- [13] T. S. Dhope, "Application of MUSIC, ESPRIT and ROOT MUSIC in DOA estimation," *Fac. Elect. Eng. Comput.*, Univ. Zagreb, Croatia, 2010.
- [14] F. Gao and A. B. Gershman, "A generalized ESPRIT approach to direction-of-arrival estimation," *IEEE Signal Process. Lett.*, vol. 12, no. 3, pp. 254–257, Mar. 2005.
- [15] P. Pal and P. P. Vaidyanathan, "Nested arrays: A novel approach to array processing with enhanced degrees of freedom," *IEEE Trans. Signal Process.*, vol. 58, no. 8, pp. 4167–4181, Aug. 2010.
- [16] P. P. Vaidyanathan and P. Pal, "Sparse sensing with co-prime samplers and arrays," *IEEE Trans. Signal Process.*, vol. 59, no. 2, pp. 573–586, Feb. 2010.
- [17] A. Moffet, "Minimum-redundancy linear arrays," *IEEE Trans. Antennas Propag.*, vol. AP-16, no. 2, pp. 172–175, Mar. 1968.
- [18] M. Wang and A. Nehorai, "Coarrays, MUSIC, and the Cramér-Rao bound," *IEEE Trans. Signal Process.*, vol. 65, no. 4, pp. 933–946, Feb. 2017.
- [19] M. Wang, Z. Zhang, and A. Nehorai, "Performance analysis of coarray-based MUSIC in the presence of sensor location errors," *IEEE Trans. Signal Process.*, vol. 66, no. 12, pp. 3074–3085, Jun. 2018.
- [20] H. Ali, S. Ahmed, M. S. Sharawi, M.-S. Alouini, and T. Y. Al-Naffouri, "Reduced complexity DOA and DOD estimation for a single moving target in bistatic MIMO radar," *Signal Process.*, vol. 166, 2020, Art. no. 107276.
- [21] J.-T. Kim, S.-H. Moon, D. S. Han, and M.-J. Cho, "Fast DOA estimation algorithm using pseudocovariance matrix," *IEEE Trans. Antennas Propag.*, vol. 53, no. 4, pp. 1346–1351, Apr. 2005.
- [22] V. Dang and O. Kilic, "Joint DOA-range-doppler tracking of moving targets based on compressive sensing," in *Proc. IEEE Antennas Propag. Soc. Int. Symp.*, 2014, pp. 141–142.
- [23] M. R. Azimi-Sadjadi, A. Pezeshki, and N. Roseveare, "Wideband DOA estimation algorithms for multiple moving sources using unattended acoustic sensors," *IEEE Trans. Aerosp. Electron. Syst.*, vol. 44, no. 4, pp. 1585–1599, Oct. 2008.
- [24] V. Malyavej, W. Kumkeaw, and M. Aorpimai, "Indoor robot localization by RSSI/IMU sensor fusion," in *Proc. 10th Int. Conf. Elect. Eng./Electron., Commun., Telecommun. Inf. Technol.*, 2013, pp. 1–6.
- [25] R. North, M. Richards, J. Cohen, N. Hoose, J. Hassard, and J. Polak, "A mobile environmental sensing system to manage transportation and urban air quality," in *Proc. IEEE Int. Symp. Circuits Syst.*, 2008, pp. 1994–1997.
- [26] S. Y. Cheung and P. P. Varaiya, "Traffic surveillance by wireless sensor networks," Ph.D. dissertation, Citeseer, 2006.

- [27] Y. Chi, L. L. Scharf, A. Pezeshki, and A. R. Calderbank, "Sensitivity to basis mismatch in compressed sensing," *IEEE Trans. Signal Process.*, vol. 59, no. 5, pp. 2182–2195, May 2011.
- [28] D. H. Chae, P. Sadeghi, and R. A. Kennedy, "Effects of basis-mismatch in compressive sampling of continuous sinusoidal signals," in *Proc. 2nd Int. Conf. Future Comput. Commun.*, vol. 2, 2010, pp. V2-739–V2-743.
- [29] M. Vetterli, P. Marziliano, and T. Blu, "Sampling signals with finite rate of innovation," *IEEE Trans. Signal Process.*, vol. 50, no. 6, pp. 1417–1428, Jun. 2002.
- [30] H. Pan, T. Blu, and M. Vetterli, "Towards generalized FRI sampling with an application to source resolution in radioastronomy," *IEEE Trans. Signal Process.*, vol. 65, no. 4, pp. 821–835, Feb. 2017.
- [31] T. Blu, P. Dragotti, M. Vetterli, P. Marziliano, and L. Coulot, "Sparse sampling of signal innovations," *IEEE Signal Process. Mag.*, vol. 25, no. 2, pp. 31–40, Mar. 2008.
- [32] F.-M. Hoffmann, P. A. Nelson, and F. M. Fazi, "DOA estimation performance with circular arrays in sound fields with finite rate of innovation," *IEEE/ACM Trans. Audio, Speech, Lang. Process.*, vol. 28, pp. 171–184, 2020.
- [33] F. Bellili, S. Affes, and A. Stéphenne, "DOA estimation for ULA systems from short data snapshots: An annihilating filter approach," in *Proc. IEEE Global. Telecommun. Conf.*, 2011, pp. 1–5.
- [34] P. J. Hayuningtyas and P. Marziliano, "Finite rate of innovation method for DOA estimation of multiple sinusoidal signals with unknown frequency components," in *Proc. 9th Eur. Radar Conf.*, 2012, pp. 115–118.
- [35] H. Pan, R. Scheibler, E. Bezzam, I. Dokmanić, and M. Vetterli, "FRIDA: FRI-based DOA estimation for arbitrary array layouts," in *Proc. IEEE Int. Conf. Acoust., Speech, Signal Process.*, 2017, pp. 3186–3190.
- [36] Y. Pan, G. Q. Luo, H. Jin, X. H. Zhang, and C. Yin, "DOA estimation with planar array via spatial finite rate of innovation reconstruction," *Signal Process.*, vol. 153, pp. 47–57, 2018.
- [37] H. Pan, "Looking beyond pixels: Theory, algorithms and applications of continuous sparse recovery," Ph.D. dissertation, IC, Lausanne, 2018.
- [38] R. Scheibler, "Rake, peel, sketch: The signal processing pipeline revisited," Ph.D. dissertation, IC, Lausanne, 2017.
- [39] M. Simeoni, A. Besson, P. Hurley, and M. Vetterli, "CPGD: Cadzow plug-and-play gradient descent for generalised FRI," *IEEE Trans. Signal Process.*, vol. 69, pp. 42–57, 2021.
- [40] R. Cohen and Y. C. Eldar, "Sparse array design via fractal geometries," *IEEE Trans. Signal Process.*, vol. 68, pp. 4797–4812, 2020.
- [41] C.-L. Liu and P. P. Vaidyanathan, "Super nested arrays: Linear sparse arrays with reduced mutual coupling—Part I: Fundamentals," *IEEE Trans. Signal Process.*, vol. 64, no. 15, pp. 3997–4012, Aug. 2016.
- [42] C. Gilliam and T. Blu, "Fitting instead of annihilation: Improved recovery of noisy FRI signals," in *Proc. IEEE Int. Conf. Acoust., Speech, Signal Process.*, 2014, pp. 51–55.
- [43] C. Gilliam and T. Blu, "Finding the minimum rate of innovation in the presence of noise," in *Proc. IEEE Int. Conf. Acoust., Speech, Signal Process.*, 2016, pp. 4019–4023.
- [44] R. Guo and T. Blu, "FRI sensing: Retrieving the trajectory of a mobile sensor from its temporal samples," *IEEE Trans. Signal Process.*, vol. 68, pp. 5533–5545, 2020.
- [45] R. Guo and T. Blu, "FRI sensing: 2D localization from 1D mobile sensor data," in *Proc. Asia-Pacific Signal Inf. Process. Assoc. Annu. Summit Conf.*, 2020, pp. 986–991.
- [46] R. Guo and T. Blu, "FRI sensing: Sampling images along unknown curves," in *Proc. IEEE Int. Conf. Acoust., Speech, Signal Process.*, 2019, pp. 5132–5136.
- [47] C. Sanathanan and J. Koerner, "Transfer function synthesis as a ratio of two complex polynomials," *IEEE Trans. Autom. Control*, vol. AC-8, no. 1, pp. 56–58, Jan. 1963.
- [48] A. K. Shaw, "Optimal design of digital IIR filters by model-fitting frequency response data," *IEEE Trans. Circuits Syst. II. Analog Digital Signal Process.*, vol. 42, no. 11, pp. 702–710, Nov. 1995.
- [49] D. H. Johnson and D. E. Dudgeon, *Array Signal Processing: Concepts and Techniques*. New York, NY, USA: Simon & Schuster, Inc., 1992.
- [50] D. G. Manolakis, V. K. Ingle, and S. M. Kogon, *Statistical and Adaptive Signal Processing: Spectral Estimation, Signal Modeling, Adaptive Filtering, and Array Processing*, Norwell, MA, USA: Artech House, Apr. 2005.
- [51] T. C. Yang, "Deconvolved conventional beamforming for a horizontal line array," *IEEE J. Ocean. Eng.*, vol. 43, no. 1, pp. 160–172, Jan. 2018.



Yongfei Li received the B.E. degree in electronic engineering from Sichuan University, Chengdu, China, in 2017. He is currently working toward the Ph.D. degree with the College of Information Science and Electronic Engineering, Zhejiang University, Hangzhou, China. His research interests include DOA estimation and signal processing.



Ruiming Guo received the B.E. degree in electronic engineering from Sichuan University, Chengdu, China, in 2017. He is currently working toward the Ph.D. degree with the Department of Electronic Engineering, Chinese University of Hong Kong, Hong Kong. His research interests include sampling theory, image, and signal processing.



Thierry Blu (Fellow, IEEE) was born in Orléans, France, in 1964. He received the Diplôme d'ingénieur from École Polytechnique, France, in 1986 and from Télécom Paris (ENST), France, in 1988, and the Ph.D. degree in electrical engineering from ENST in 1996, with a study on iterated rational filterbanks, applied to wideband audio coding.

From 1998 and 2007, he was with the Biomedical Imaging Group, Swiss Federal Institute of Technology, Lausanne, Switzerland. He is currently a Professor with the Department of Electronic Engineering,

The Chinese University of Hong Kong, Hong Kong. His research interests include wavelets, approximation and sampling theory, sparse representations, image denoising, biomedical imaging, optics, and wave propagation.

Dr. Blu was the recipient of two best paper awards from the IEEE Signal Processing Society in 2003 and 2006. He is also coauthor of a paper that received the Young Author Best Paper Award in 2009 from IEEE Signal Processing Society.

He has been a member of the IEEE Signal Processing Theory and Methods Technical Committee in 2008–2013, and an Associate Editor for the IEEE TRANSACTIONS ON IMAGE PROCESSING in 2002–2006, the IEEE TRANSACTIONS ON SIGNAL PROCESSING in 2006–2010, and *Signal Processing* in 2008–2011. He is currently on the board of *EURASIP Journal on Image and Video Processing* and *SIAM Journal on Imaging Sciences*, and a Member of the IEEE Bio Imaging and Signal Processing Technical Committee.



Hangfang Zhao received the B.E. degree in electronic engineering from Xidian University, Xi'an, China, in 1991, the M.E. degree in underwater engineering from Harbin Engineering University, Harbin, China, in 1997, and the Ph.D. degree in communication and information systems from Zhejiang University, Hangzhou, China, in 2010. From 1991 to 2012, she was with Hangzhou Applied Acoustics Research Institute, Hangzhou, China, where she conducted research in acoustic signal processing and acoustic engineering. In 2012, she joined Zhejiang University,

where she is currently a Professor with the Department of Information Science and Electronic Engineering. Her research interests include array signal processing, acoustic tomography and acoustic imaging, and robust signal processing in uncertain environments.